International Conference on Mathematics, Computational Methods & Reactor Physics (M&C 2009)
Saratoga Springs, New York, May 3-7, 2009, on CD-ROM, American Nuclear Society, LaGrange Park, IL (2009)

HIGH-ORDER METHOD OF CHARACTERISTICS FOR 2-D UNSTRUCTURED MESHES

Emiliano Masiello, Roberto Clemente, Simone Santandrea
Commissariat à l'Energie Atomique
Direction de l'Energie Nucléaire
Service d'Etudes de Réacteurs et de Mathématiques Appliquées
CEA de Saclay, DEN/DANS/DM2S/SERMA/LTSD
91190 Gif sur Yvette, CEDEX France
emiliano.masiello@cea.fr, roberto.clemente@cea.fr,
simone.santandrea@cea.fr

ABSTRACT

In this work, a high-order flux expansion is applied to the method of long characteristics. We describe two different strategies to handle the discretized form of the transport equation. For both methods, a comparison of the performances is presented starting from the constant approximation up to the fourth order approximation. A 2-D heterogeneous source problem is analyzed. The results are presented and discussed to emphasize the interest for such methods. Principally, the observed spatial convergence rate is scanned. The significant figure of the analysis is that high-order spatial expansions allow for the treatment of coarser meshes while preserving the same accuracy of the step characteristics with finer grids. Also, we show that, for a given error tolerance, such an advantage is straightforward translated in terms of less computational cost for both storage requirement and CPU time.

Key Words: method of characteristics, high-order spatial expansion

1. INTRODUCTION

The method of characteristics (MOC) is one of the most versatile methods used for 2D industrial lattice calculations. Thanks to the trajectory-based sweeping, it allows for the treatment of unstructured and non-conforming meshes without any restriction. However, in spite of its popularity, the MOC suffers at least of one drawback: the step approximation of the source.

In this work, two high order methods of characteristics are presented. Both methods are derived by expanding the angular moments of the flux within a homogeneous region on locally defined polynomial bases up to the fourth order polynomial. Also, both methods share the same transmission equation to propagate the uncollided flux throughout the domain along a parallel set of trajectory per each discrete direction. The main difference between the two methods is in the way the internal spatial moments of the angular flux are computed.

The first method relies on the projection of the integral transport equation on the locally defined test functions used to expand the source. Taking profit of the explicit nature of the integral formulation, no assumption is made on the spatial distribution of the angular flux. However, even if the angular flux is not explicitly expanded, such a numerical approximation leads to a coherent

method, i.e. a method in which the spatial approximations of the angular flux is the same as that of the angular moments of the flux.

The second method is based on the projection of the differential transport equation along the trajectory segment. In this case, an assumption on the spatial behavior of the angular flux is strictly necessary for solving the discretized system. For this method, we have chosen to experiment two different spatial representations respectively for the angular flux and for the angular moments. More precisely, the angular flux is expanded on a trajectory-dependent linear Lagrangian base, while the angular moments are polynomially expanded on the region. Such an approximation leads to an incoherent method, in particular, in our implementation the second method becomes incoherent when the source has a parabolic, or cubic, or fourth order expansion while the angular flux remains linear on trajectories.

The formalism of the two methods has the generality to be extended to multidimensional geometry. As in the standard step MOC, the domain is swept trajectory by trajectory for the accumulation of the leakage contribution through the regions. The trajectory contributions are numerically integrated on the spatial transverse coordinate and on the angular coordinate providing thus the calculation of the angular moments of the source.

The rest of the paper is organized as follows. In the next Section we give some basic assumptions shared by the two methods. In Section 3 and 4 the coherent and the incoherent methods will be discussed, while an analysis of the numerical spatial convergence test on the Azmy test problem will be presented in Section 5. Finally, we conclude the paper with considerations and further remarks in Section 6.

2. PRELIMINARIES

Our purpose is to derive two numerical methods for the solution of the discrete ordinates transport equation for a given energy group. We suppose to deal with the unstructured partition of the domain, $D = \bigcup_{r=1,R} D_r$, where D_r are the homogenous region and r is the region index. The flux along a trajectory intersecting D_r can be described by the integral equation

$$\begin{aligned} \psi(\mathbf{r},\mathbf{\Omega}) &= \psi^-_{rt} e^{-\Sigma_r l} + (Kq)(\mathbf{r},\mathbf{\Omega}), \\ q(\mathbf{r},\mathbf{\Omega}) &= \sum_{h=1,H} \Sigma_{rh} A_h(\mathbf{\Omega}) \phi_h(\mathbf{r}) + S(\mathbf{r},\mathbf{\Omega}) \quad \forall (\mathbf{r},\mathbf{\Omega}) \in D_r \times S_N. \end{aligned} \tag{1}$$

Here, K is the operator $(Kq)(\mathbf{r},\mathbf{\Omega}) = \int_0^l dx\, q(\mathbf{r}_{rt} + x\mathbf{\Omega},\mathbf{\Omega}) e^{-\Sigma_r (l-x)}$, $\psi^-_{rt} = \psi(\mathbf{r}_{rt},\mathbf{\Omega})$ is the incoming flux relative to the hanging surface point $\mathbf{r}_{rt}$ of the trajectory, while $\mathbf{r} = \mathbf{r}_{rt} + l\mathbf{\Omega}$ is the spatial coordinates with respect to the local coordinate system of D_r. $S(\mathbf{r},\mathbf{\Omega})$ is the group source, which includes neutrons input to the group due to inhomogeneous, fission and scattering source. One takes $S(\mathbf{r},\mathbf{\Omega})$ to be known for the previous outer iteration, while the self scattering

contribution in $q(\mathbf{r}, \mathbf{\Omega})$ is updated at each inner iteration. The scattering source expansion is expressed for simplicity with the single index h. A quadrature rule is used to perform the angular integration to update the angular moments $\phi_h(\mathbf{r})$,

$$\phi_h(\mathbf{r}) = \int_{4\pi} d\mathbf{\Omega}\, A_h(\mathbf{\Omega})\psi(\mathbf{r}, \mathbf{\Omega}), \tag{2}$$

where $A_h(\mathbf{\Omega})$ are the spherical harmonics. For the rest of the paper, the angular integral (2) should be understood as angular quadrature. Eq. (1) is utilized in the MOC to propagate the flux throughout the domain, while the neutron balance is preserved by averaging the differential transport equation

$$(\mathbf{\Omega} \cdot \boldsymbol{\nabla} + \Sigma_r)\psi(\mathbf{r}, \mathbf{\Omega}) = q(\mathbf{r}, \mathbf{\Omega}) \tag{3}$$

along each trajectory.

The methods proposed in this paper are formally based on the Petrov-Galerkin projection technique and, therefore, we provide the definition of a suitable scalar product for the MOC formalism. [1], [2] For this purpose, we have to deal with the angular dependent discretization induced by the trajectory tracking. More precisely, the trajectory tracking leads to the partition $D \simeq \bigcup_{r=1,R} D_{r,\mathbf{\Omega}}$, where $D_{r,\mathbf{\Omega}}$ is the tracking-induced discretization of the region r and it is of course angular-dependent. By defining $w_{\perp,t}$ as the weight associated to a trajectory t and l_{rt} as the segments relative to the trajectory t across the region r, we can define a numerical scalar product on $D_{r,\mathbf{\Omega}} = \bigcup_{t \cap r,\ t \| \mathbf{\Omega}} w_{\perp,t} l_{rt}$ as

$$(f, g)_{\mathbf{\Omega}} = \int_{D_{r,\mathbf{\Omega}}} d\mathbf{r}\ (fg)(\mathbf{r}_{rt} + x\mathbf{\Omega}) = \sum_{t \cap r,\ t \| \mathbf{\Omega}} w_{\perp,t}(f, g)_t(\mathbf{r}_{rt}, l_{rt}, \mathbf{\Omega}), \tag{4}$$

where $f(\mathbf{r})$ and $g(\mathbf{r})$ are two generic functions, while

$$(f, g)_t(\mathbf{r}_{rt}, l_{rt}, \mathbf{\Omega}) = \int_0^{l_{rt}} dx (fg)(\mathbf{r}_{rt} + x\mathbf{\Omega}),\ \ \forall\, t \| \mathbf{\Omega}, \tag{5}$$

is the integral along the trajectory segments l_{rt}. The numerical scalar product (4) is angular dependent, thus, it can not be used to compute the spatial moments of $\phi_h(\mathbf{r})$. For that reason, we define the volume scalar as the average value of $(f, g)_{\mathbf{\Omega}}$ over the unit sphere,

$$(f, g) = \frac{1}{4\pi} \int_{4\pi} d\mathbf{\Omega}(f, g)_{\mathbf{\Omega}}, \tag{6}$$

where the angular integration is performed numerically with the quadrature formula provided by the discrete ordinates.

To complete the definition of the Petrov-Galerkin projector, we have to specify the trial function for $\phi_h(\mathbf{r})$. In our implementation we have used the monomial base

$$\overrightarrow{P}_r(\mathbf{r}) = \{1, x,\ y, xy, x^2,\ y^2, x^2y, xy^2, x^3,\ y^3, x^2y^2, x^3y,\ xy^3, x^4,\ y^4\}^{\intercal}. \tag{7}$$

which is locally defined in D_r. For practical reasons, we have centered the local system of D_r in its baricenter. This implies that, regardless of the shape of the region, the linear components are orthogonal to the constant component.

The first step for the discretization is the spatial expansion of the angular moments on $\overrightarrow{P}_r(\mathbf{r})$,

$$\phi_h(\mathbf{r}) \simeq \overrightarrow{P}_r(\mathbf{r}) \cdot \overrightarrow{\phi}_{h,r} \quad \mathbf{r} \in D_r,\ h = 1, H, \tag{8}$$

which implies also $q(\mathbf{r}, \mathbf{\Omega}) \simeq \overrightarrow{P}_r(\mathbf{r}) \cdot \overrightarrow{q}_r(\mathbf{\Omega})$. The spatial moments $\overrightarrow{\phi}_{h,r}$ are computed by equating the later approximation to the definition (2)

$$\begin{aligned} (\overrightarrow{P}_r, \overrightarrow{P}_r)\overrightarrow{\phi}_{h,r} &= (\overrightarrow{P}_r, \phi_h) = \int_{4\pi} d\mathbf{\Omega}\ A_h(\mathbf{\Omega})(\overrightarrow{P}_r, \psi)_{\mathbf{\Omega}}(\mathbf{\Omega}), \\ h &= 1, H \end{aligned} \tag{9}$$

Inserting the latter approximation in Eq. (1) and extending the flux to the point $\mathbf{r}_{rt} + l_{rt}\mathbf{\Omega}$, one obtains

$$\psi^+_{rt} = \psi^-_{rt} e^{-\tau_{rt}} + \overrightarrow{F}_{rt} \cdot \overrightarrow{q}_r, \tag{10}$$

which is the propagation equation for the outgoing flux $\psi^+_{rt} = \psi(\mathbf{r}_{rt} + l_{rt}\mathbf{\Omega}, \mathbf{\Omega})$. Here, τ_{rt} is the optical thickness of the trajectory segment and

$$\overrightarrow{F}_{rt} = \overrightarrow{F}(\mathbf{r}_{rt}, l_{rt}, \mathbf{\Omega}) = e^{-\tau_{rt}}(e^{\tau}, \overrightarrow{P}_r)_t\ . \tag{11}$$

In the following sections we propose two different strategies for the calculation of the spatial moments of the angular flux on a trajectory, which are defined by the projection

$$\overrightarrow{\psi}_{rt}(\mathbf{\Omega}) = (\overrightarrow{P}_r, \psi)_t(\mathbf{\Omega}) \tag{12}$$

For both methods, Eq. (10) is used to propagate the flux throughout the domain allowing for the computation of the streaming term on each region.

3. COHERENT METHOD

The first method is based on the projection of the integral transport equation on the subspace spanned by $\overrightarrow{P}_r(\mathbf{r})$. Substituting Eq. (1) in the definition (12) one obtains

$$\overrightarrow{\psi}_{rt} = \overrightarrow{G}_{rt}\psi^-_{rt} + \overline{\overline{H}}_{rt} \cdot \overrightarrow{q}_r \tag{13}$$

where the vector $\overrightarrow{G}_{rt}$ and the matrix $\overline{\overline{H}}_{rt}$ are respectively the exponential functions

$$\overrightarrow{G}_{rt} = G(\mathbf{r}_{rt}, l_{rt}, \mathbf{\Omega}) = (\overrightarrow{P}_r, e^{-\Sigma_r l})_t, \tag{14}$$

$$\overline{\overline{H}}_{rt} = H(\mathbf{r}_{rt}, l_{rt}, \mathbf{\Omega}) = (\overrightarrow{P}_r, K\overrightarrow{P}_r)_t. \tag{15}$$

Eq. (13) is used during the sweeping to cumulate the trajectory contributions to the spatial moments of the angular flux

$$\overrightarrow{\psi}_r(\mathbf{\Omega}) = (\overrightarrow{P}_r, \psi)_{\mathbf{\Omega}} = \sum_{t \cap r,\ t \| \mathbf{\Omega}} w_{\perp,t}\overrightarrow{\psi}_{rt}(\mathbf{\Omega}). \tag{16}$$

The spatial moments $\overrightarrow{\phi}_{h,r}$ are computed using Eq. (9)

$$\overrightarrow{\phi}_{h,r} = \overline{\overline{M}}_r^{-1} \int_{4\pi} d\mathbf{\Omega}\; A_h(\mathbf{\Omega})\, \overrightarrow{\psi}_r(\mathbf{\Omega}) \tag{17}$$

where $\overline{\overline{M}}_r = (\overrightarrow{P}_r, \overrightarrow{P}_r)$.

In this method no approximation of the angular flux is necessary; this is a prerogative of the integral transport equation which gives explicitly the distribution of the uncollided neutrons along a trajectory. As a consequence, in the limit of the approximation (8), Eq. (13) is exact. Moreover, taking the correct Taylor expansion for coefficients (11), (14) and (15), the projection of the integral transport equation does not suffer from round-off errors (e.g. in problem with voided regions).

4. INCOHERENT METHOD

For the calculation of the spatial moments $\overrightarrow{\psi}_{rt}(\mathbf{\Omega})$, the second method makes use of the projection of the differential transport equation, Eq. (3). Another big difference with the coherent method is that, here, two different supports are exploited to represent respectively the angular moments and the angular flux. More precisely, as for the first method, the angular moments $\phi_h(\mathbf{r})$ are developed on D_r using $\overrightarrow{P}_r(\mathbf{r})$ as trial function, i.e. Eq. (8). On the other hand, the angular flux $\psi(\mathbf{r}, \mathbf{\Omega})$ is expanded on $D_{r,\mathbf{\Omega}}$, which is the tracking-induced discretization of D_r, and the spatial distribution is approximated with linear Lagrangian base functions locally defined on each trajectory. In particular,

$$\overrightarrow{f}_{rt}(l) = \frac{1}{l_{rt}}\{l_{rt} - l, l\}^\intercal \tag{18}$$

is the linear characteristic function for a trajectory t crossing the region r and, therefore, one can expand $\psi(\mathbf{r}, \mathbf{\Omega})$ as

$$\psi(\mathbf{r} = \mathbf{r}_{rt} + l\mathbf{\Omega}, \mathbf{\Omega}) \simeq \sum_{t \cap r,\; t \| \mathbf{\Omega}} \overrightarrow{f}_{rt}(l) \cdot \overrightarrow{\psi}_{rt}(\mathbf{r}_{rt}, \mathbf{\Omega}) \quad \mathbf{r} \in D_{r,\mathbf{\Omega}} \tag{19}$$

where $\overrightarrow{\psi}_{rt}(\mathbf{r}_{rt}, \mathbf{\Omega}) = \{\psi_{rt}^{v,-} = \psi(\mathbf{r}_{rt}, \mathbf{\Omega}), \psi_{rt}^{v,+} = \psi(\mathbf{r}_{rt} + l_{rt}\mathbf{\Omega}, \mathbf{\Omega})\}^\intercal$ becomes the vector containing the collocative value of the flux at the hanging points of the trajectory. We pointout that these values, $\psi_{rt}^{v,\pm}$, are different from the incoming/outgoing flux $\psi_{rt}^{\pm}$, we have indicated with the superscript v the flux values relative to the volume expansion. In the approximation (19), the angular flux is considered piecewise-constant on the perpendicular surface while it is expanded on the linear base along the trajectory coordinate l.

Introducing the expansion (19) in the differential equation (3) and by projecting on $\overrightarrow{f}_{rt}(l)$ one obtains

$$\overline{\overline{K}}_{rt}\, \overrightarrow{\psi}_{rt} = \overline{\overline{M}}_{rt}\, \overrightarrow{q}_r - (\overrightarrow{f}^{+}_{rt}\psi^{+}_{rt} - \overrightarrow{f}^{-}_{rt}\psi^{-}_{rt}), \tag{20}$$

where $\overline{\overline{K}}_{rt}$ is the "stiffness" matrix,

$$\overline{\overline{K}}_{rt} = \overline{\overline{K}}(\mathbf{r}_{rt}, l_{rt}, \mathbf{\Omega}) = -(\partial_l \overrightarrow{f}_{rt}, \overrightarrow{f}_{rt})_t + \Sigma_r(\overrightarrow{f}_{rt}, \overrightarrow{f}_{rt})_t,$$

while $\overline{\overline{M}}_{rt}$ is the mass matrix,

$$\overline{\overline{M}}_{rt} = \overline{\overline{M}}(\mathbf{r}_{rt}, l_{rt}, \mathbf{\Omega}) = (\overrightarrow{f}_{rt}, \overrightarrow{P}_r)_t,$$

and $\overrightarrow{f}^{-}_{rt} = \overrightarrow{f}_{rt}(0) = \{1,0\}^{\intercal}$ and $\overrightarrow{f}^{+}_{rt} = \overrightarrow{f}_{rt}(l_{rt}) = \{0,1\}^{\intercal}$. The projection (20) is very similar to the linear discontinuous finite element method in slab geometry, the difference is on the boundary terms, i.e. the second term on the R.H.S. of the equation, where the transmitted flux $\psi^{\pm}_{rt}$ are used to compute the boundary integral of the streaming term.

Using Eq. (16) and the scalar product (4), one obtains the spatial moments on $D_{r,\mathbf{\Omega}}$ of the angular flux,

$$\overrightarrow{\psi}_r(\mathbf{\Omega}) = (\overrightarrow{P}_r, \psi)_{\mathbf{\Omega}} = \sum_{t \cap r,\ t \| \mathbf{\Omega}} w_{\perp,t} \overline{\overline{M}}^{\intercal}_{rt} \overrightarrow{\psi}_{rt}(\mathbf{\Omega}_d). \tag{21}$$

As for the first method, Eq. (17) is used to update the angular moments of the flux to compute the new source.

5. SWEEPING AND STORAGE REQUIREMENTS

The methods here proposed have been implemented on the prototype version of the MOC solver for unstructured geometry used in our laboratory, namely TDT (Two-Dimensional Transport solver). [6] [7] For both method, the user can choose the degree of the polynomial expansion of the source up to the fourth order. In this section we pointout two significant differences between the coherent method and the incoherent method in terms of implementation, in particular, for the sweeping algorithm and for the storage requirements.

For the coherent method, the coefficient arrays $\overrightarrow{F}$, $\overrightarrow{G}$, and the matrix $\overline{\overline{H}}$ are stored for each trajectory segment and for each energy group before the start of the iterative process. The following relations,

$$\begin{aligned} \overrightarrow{F}(\mathbf{r}_{rt}, l_{rt}, \mathbf{\Omega}) &= \overrightarrow{G}(\mathbf{r}_{rt} + l_{rt}\mathbf{\Omega}, l_{rt}, -\mathbf{\Omega}) \\ \overline{\overline{H}}(\mathbf{r}_{rt}, l_{rt}, \mathbf{\Omega}) &= \overline{\overline{H}}^{\intercal}(\mathbf{r}_{rt} + l_{rt}\mathbf{\Omega}, l_{rt}, -\mathbf{\Omega}) \end{aligned}$$

which reflect the reciprocity of the Green functions, helps to reduce of one-half the amount of stored data. This means that the total container array length (CAL) for the first method is equal to

$$CAL = N_m(2 + N_m) \times N_{trk} \times N_g, \tag{22}$$

where N_m is the number of moments of the source,

$$N_m = \begin{cases} 1 & \text{for constant,} \\ 3 & \text{for linear,} \\ 6 & \text{for parabolic,} \\ 10 & \text{for cubic,} \\ 15 & \text{for 4th order,} \end{cases}$$

while N_{trk} and N_g are respectively the number of trajectory segments and the number of energy groups. Once $\overrightarrow{F}$, $\overrightarrow{G}$, and $\overline{\overline{H}}$ are computed and stored, Eqs. (10) and (17) are solved

simultaneously for each trajectory segment. For this method, the CAL can explode dramatically as the spatial order increases.

For the second method, only the coefficient array $\overrightarrow{F}$ is stored and, therefore, the CAL reduces to

$$CAL = 2N_m \times N_{trk} \times N_g,$$

where the forward ($\mathbf{\Omega}$) and backward ($-\mathbf{\Omega}$) coefficients are here taken into account. On the other hand, the second method has an overhead of arithmetic operations per sweeping. The transmission equation remains the same as for the first method, while the balance equation, Eq. (20), is solved on the fly. In particular, the inverse of the stiffness matrix $\overline{\overline{K}}_{rt}$, which is a simple 2×2 matrix, is recalculated during the sweeping. Moreover, the calculation of the region-wise spatial moments $\overrightarrow{\psi}_r(\mathbf{\Omega})$, Eq. (21), implies the application for each trajectory segments of the matrix $\overline{\overline{M}}_{rt}^{\mathsf{T}}$.

6. SPATIAL CONVERGENCE TEST

We have numerically tested the spatial convergence of the method on a 2-D one-group source problem with isotropic scattering presented in reference [3]. The problem consists of a square source of 10 cm per side imbedded in a square of 20 cm per side of absorber material with void boundary conditions on the external surfaces. The total cross section, the scattering cross sections and the source are respectively $\Sigma = 1$, $\Sigma_s = 0.5$, $S = 1$ for the source material and $\Sigma = 2$, $\Sigma_s = 0.1$, $S = 0$ for the absorber material. Taking profit of the shape of the geometry, the dimension of the problem is reduced to 1/4 of the real geometry using specular boundary conditions on the left and bottom sides of the square. A product quadrature formula consisting of 16 discrete directions (8 azimuthal angles and 2 polar angles) has been used for the angular discretization and the trajectory spacing being used for all run cases is of 10^{-3} cm for a total of $\sim 2 \times 10^4$ trajectories per azimuthal angle. [6]

We have checked the numerical spatial convergence on the average fluxes in the bottom-left square (source material), the bottom-right square and upper-right square (absorber material). The Tables I and II show results respectively for the coherent and incoherent methods. For each spatial order, we have run cases by progressively increasing the $2^M \times 2^M$ Cartesian mesh, with the progression $M = 1, 2, 3, 4, 5, 6, 7$, until reaching an accuracy on the fourth significant figure of the flux values for the three checked zones. A 10^{-5} relative error precision on the region-wise convergence of the scalar flux has been used as stopping criterion of source iterations.

This test shows the interest of using a high-order flux expansion in a coarse grid. High-order flux expansion guarantees the same accuracy as a low-order expansion in a finer grid while requiring less computing time and, for very heterogeneous problems, less data storage. For instance, to the same order of accuracy, both method with a linear expansion on a $2^5 \times 2^5$ grid, or a parabolic expansion on a $2^4 \times 2^4$, or a cubic expansion on a $2^3 \times 2^3$ require between $\sim$30%$\div$60% less computing time than a constant expansion on a $2^7 \times 2^7$ grid. On the other hand, the fourth order expansion is the only approximation for which the computing cost explodes.

The second significant aspect is that the coherent and the incoherent methods exhibit the same behavior for constant and linear approximation. Even if the region-wise convergence is slightly different, the two methods have the same spatial convergence rate in the L2-norm. We present

Table I. Results for the numerical spatial convergence test obtained with the coherent method. n = 0 constant, n = 1 linear, n = 2 parabolic, n = 3 cubic, n = 4 fourth order. M = exponent for calculating the number of mesh. BR = average flux in the bottom-right square, BL = average flux in the bottom-left square, TR = average flux in the top-right square. CAL = container array length, N. It. = number of iterations, CPU = CPU time

n	M	BL	BR$\times 10^2$	TR$\times 10^3$	CAL (Mo)	N. It.	CPU (s)
0	1	1.644	4.549	2.327	1.2	16	2.7
	2	1.655	4.424	2.185	2.5	16	5.2
	3	1.667	4.270	2.029	5.0	16	10.6
	4	1.676	4.164	1.942	10.0	16	20.3
	5	1.679	4.116	1.916	20.0	17	43.5
	6	1.681	4.100	1.911	40.1	17	85.6
	7	**1.681**	**4.095**	**1.911**	**80.2**	**17**	**163.8**
1	1	1.666	4.305	2.039	6.2	16	4.9
	2	1.676	4.173	1.926	12.5	18	10.8
	3	1.680	4.114	1.903	25.0	17	20.4
	4	1.681	4.098	1.907	50.1	17	40.2
	5	**1.681**	**4.095**	**1.910**	**100.3**	**17**	**80.5**
2	1	1.676	4.156	1.899	20;0	16	10.6
	2	1.681	4.109	1.896	40.0	18	23.8
	3	1.681	4.096	1.905	80.2	17	45.4
	4	**1.681**	**4.094**	**1.910**	**160.5**	**17**	**90.3**
3	1	1.680	4.117	1.894	50.1	16	22.7
	2	1.681	4.097	1.903	100.3	17	48.4
	3	**1.681**	**4.094**	**1.910**	**200.6**	**17**	**103.2**
4	1	1.681	4.099	1.896	106.6	16	44.8
	2	**1.681**	**4.094**	**1.910**	**213.2**	**16**	**177.3**

Table II. Results for the numerical spatial convergence test obtained with the incoherent method. n = 0 constant, n = 1 linear, n = 2 parabolic, n = 3 cubic, n = 4 fourth order. M = exponent for calculating the number of mesh. BR = average flux in the bottom-right square, BL = average flux in the bottom-left square, TR = average flux in the top-right square. CAL = container array length, N. It. = number of iterations, CPU = CPU time

n	M	BL	BR$\times 10^2$	TR$\times 10^3$	CAL (Mo)	N. It.	CPU (s)
0	1	1.644	4.549	2.327	0.6	16	3.9
	2	1.655	4.424	2.185	1.3	16	7.8
	3	1.667	4.270	2.029	2.5	16	15.3
	4	1.676	4.164	1.942	5.1	16	30.7
	5	1.679	4.116	1.916	10.1	17	63.9
	6	1.681	4.100	1.911	20.0	17	127.6
	7	**1.681**	**4.095**	**1.911**	**40.1**	**17**	**247.3**
1	1	1.666	4.305	2.039	1.2	16	6.7
	2	1.676	4.173	1.926	2.5	18	15.2
	3	1.680	4.114	1.903	5.0	17	28.5
	4	1.681	4.098	1.907	10.2	17	57.0
	5	**1.681**	**4.095**	**1.910**	**20.0**	**17**	**113.8**
2	1	1.669	4.249	1.957	2.9	16	12.4
	2	1.678	4.137	1.905	5.7	16	24.9
	3	1.681	4.101	1.905	11.5	17	53.3
	4	**1.681**	**4.095**	**1.909**	**23.0**	**17**	**107.6**
3	1	1.671	4.227	1.970	4.6	16	22.9
	2	1.678	4.129	1.915	9.1	16	45.9
	3	1.681	4.100	1.908	18.2	17	102.5
	4	**1.681**	**4.095**	**1.909**	**40.7**	**17**	**189.8**
4	1	1.671	4.225	1.934	6.7	16	41.2
	2	1.679	4.128	1.908	13.3	16	82.6
	3	1.681	4.100	1.908	26.7	17	356.0
	4	**1.681**	**4.095**	**1.910**	**52.3**	**16**	**983.3**

here an heuristic argument to justify such a result for the linear expansion, since for constant approximation it is trivial. If we write the linear monomial base $\overrightarrow{P}_r(\mathbf{r}) = \{1, x, y\}$ on a point belonging to the trajectory t in a direction $\mathbf{\Omega}$, we obtains

$$\overrightarrow{P}_r(\mathbf{r} = \mathbf{r}_{rt} + l\mathbf{\Omega}) = \overline{\overline{D}}_{rt} l_{rt} \overrightarrow{f}_{rt}(l),$$

where $\overline{\overline{D}}_{rt} = \overline{\overline{D}}(\mathbf{r}_{rt}, \mathbf{\Omega})$ is the constant coefficients matrix resulting from the linear transformation $x = x_{rt} + l\Omega_x$, and $y = y_{rt} + l\Omega_y$, while $\overrightarrow{f}_{rt}(l)$ is the linear Lagrangian base, Eq. (18), used for the angular flux expansion in the incoherent method. Since the $\overrightarrow{P}_r(\mathbf{r})$ components are linear combination of $\overrightarrow{f}_{rt}(l)$ components, both bases span the same subspace on the trajectory. Moreover, if the expansion

$$\psi(\mathbf{r}, \mathbf{\Omega}) \simeq \overrightarrow{P}_r(\mathbf{r}) \cdot \overrightarrow{\psi}_r(\mathbf{\Omega}) = \sum_{t \cap r,\ t \| \mathbf{\Omega}} \overline{\overline{D}}_r(\mathbf{r}_{rt}, \mathbf{\Omega}) l_{rt} \overrightarrow{f}_{rt}(l) \cdot \overrightarrow{\psi}^*_{rt}(\mathbf{r}_{rt}, \mathbf{\Omega}) \quad \mathbf{r} \in D_r \tag{23}$$

holds, the projection (13) of the integral transport equation is analytically equivalent to

$$\overline{\overline{K}}_{rt} \overline{\overline{D}}_{rt} l_{rt} \overrightarrow{\psi}^*_{rt}(\mathbf{\Omega}) = \overline{\overline{M}}_{rt} \overrightarrow{q}_r - (\overrightarrow{f}^{+}_{rt} \psi^{+}_{rt} - \overrightarrow{f}^{-}_{rt} \psi^{-}_{rt}),$$

which is the projected differential transport equation used for the incoherent method, i.e. Eq. (20) with $\overrightarrow{\psi}_{rt}(\mathbf{\Omega}) = \overline{\overline{D}}_{rt} l_{rt} \overrightarrow{\psi}^*_{rt}(\mathbf{\Omega})$. Since $\overrightarrow{\psi}_{rt}(\mathbf{\Omega})$ is a linear combination of $\overrightarrow{\psi}^*_{rt}(\mathbf{\Omega})$ the linear incoherent method is actually equivalent to the linear coherent method if the expansion (3) holds.

In Fig. 1 and Fig. 2 are depicted the linear fittings of the L2-norm errors for the coherent method and the incoherent method in all the spatial order here analyzed. Table III shows that the convergence order for the parabolic, cubic and 4th order expansion of the incoherent method is degraded with respect to the same orders of the coherent method. However, Fig. 2 shows that the absolute magnitude of the error for the parabolic, cubic and 4th order expansions is less than the constant and linear order. Moreover, the parabolic, cubic and 4th order expansions of the incoherent method are less computationally demanding with respect to the same expansion order of the coherent method. In fact, the sweeping overhead caused by the on-the-fly solution of Eq. (13) discussed in the previous Section is partially compensated by the fact that the expanded angular flux remains linear on the trajectory. Therefore, even if the spatial convergence is degraded, such method could be a good compromise between accuracy and computational cost.

Also, we underline that a theoretical study of the spatial convergence order for constant and linear characteristics method in slab homogeneous geometry has been performed in Ref. [4]. This work shows that constant and linear characteristics exhibit respectively second and fourth order convergence. Such results are supported also by numerical simulations. However, theoretical evaluations of the convergence rate are based on the regularity of the flux, which seems optimistic in most practical applications. In the case of multidimensional heterogeneous geometry as the problem here analyzed, the theoretical convergence rate is hardly predictable because the flux is no longer an analytical function. Moreover, the observed convergence rates of Table III suffer from errors introduced by the numerical transverse integration, i.e. Eqs. (16) and (21). As suggested and detailed in Ref. [5], such an error is of the order of the trajectory spacing h, thus, a conservative criterion to preserve the theoretical spatial convergence rate is to choose $h \sim \Delta^k$, where k is the theoretical convergence order and Δ is the average diameter of regions. We argue

Table III. Numerical observed spatial convergence order obtained by linearly fitting the L2-norm error. CM = convergence order for the Coherent Method, IM = convergence order for the Incoherent Method

	CM	**IM**
constant	0.72	0.72
linear	1.47	1.47
parabolic	1.73	1.16
cubic	2.14	1.08
4th order	2.17	1.08

that the numerical spacing used in this test, $h = 10^{-3}cm$, could especially pollute the solution obtained with fine grid and high-order flux expansions. On the other hand, the previous criterion is unsuitable for realistic lattice calculations.

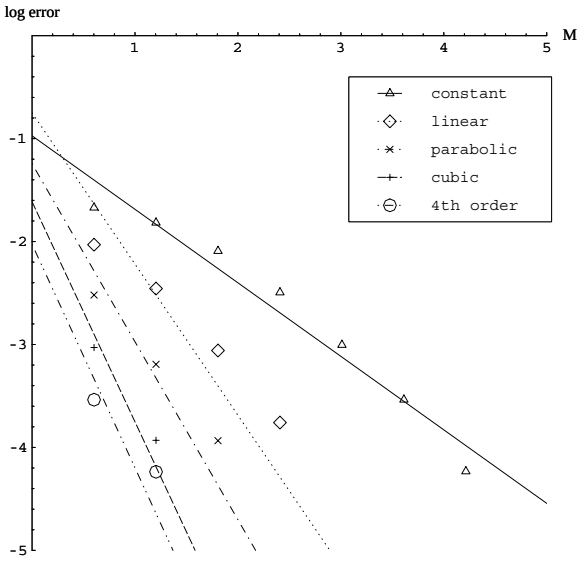

Figure 1. Coherent method: linear fitting of the L2-norm error for the constant, linear, cubic, and 4th order spatial expansion. Here, M is the exponent which gives the number of regions, i.e. $2^M \times 2^M$.

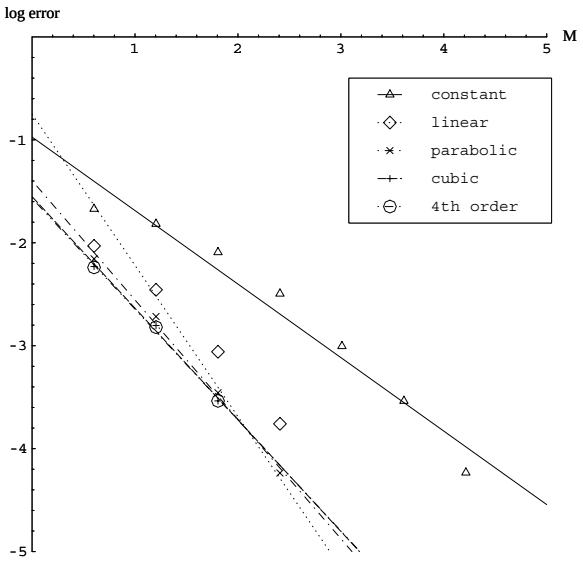

Figure 2. Incoherent method: linear fitting of the L2-norm error for the constant, linear, cubic, and 4th order spatial expansion. Here, M is the exponent which gives the number of regions, i.e. $2^M \times 2^M$.

7. CONCLUSIONS AND FURTHER REMARKS

Following a projective technique framework, we have presented in this paper a numerical application of two higher order methods for long characteristics. The interest of such methods in a coarser grid is twofold. First, for a given accuracy, a coarser grid with high order approximation is less memory demanding than a finer grid with step approximation. Second, a coarser grid allows for a coarsening of the spatial quadrature for the transverse integration Eq. (4), which implies less number of trajectories and, therefore, less data to be processed. We have not presented here a sensitivity study on trajectory spacing, but our numerical experience shows that the higher order flux expansion allows for a degradation of the transverse integration. For these reasons, the application of higher order MOC results less computationally costing.

We have numerically checked the equivalence between the integral and the differential formulation for the constant and linear approximation and we have appended a heuristic argument to justify this result. However, the incoherent method, resulting from the projection of the differential equation, shows a degradation of the spatial convergence rate for the parabolic, the cubic and the fourth order approximations. This is mainly due to the linear expansion of the angular flux which leads to a spurious method when the source is high order expanded, i.e. more than linear. This fixed choice we have made for the differential formulation has two motivations. First, the on-the-fly solution of Eq. (20) becomes unpractical for orders higher than linear. Moreover, the incoherent method is less memory demanding and computationally costing than the coherent method and, even if the spatial convergence is degraded, it guarantees a sensible reduction of the local error.

The results presented in the previous Section have been obtained with a plug-and-play implementation of the methods in the prototype version of the TDT MOC solver. [6] [7] We have given any attention to the informatics optimization to minimize the computational time. Further, we obviously believe that an acceleration technique for the source iterations together with an optimization of the computational algorithm is strictly necessary to promote such methods to realistic lattice calculation.

REFERENCES

[1] V. S. Vladimirov, *Mathematical Problems in the One-Velocity Theory of Particle Transport*, Atomic Energy of Canada Ltd., Chalk River, Report AECL-1661 (1963).

[2] J. J. Duderstadt, W. R. Martin, *Transport Theory*, Wiley and Sons, New York (1979).

[3] Y. Y. Azmy, 'The Weighted Diamond-Difference Form of Nodal Transport Methods,' *Nucl. Sci. and Eng.,* **98**, 29-40 (1988).

[4] E. W. Larsen, W. F. Miller, Jr, "Convergence Rates of Spatial Difference Equations for Discrete-Ordinates Neutron Transport Equations in Slab Geometry," *Nucl. Sci. and Eng.,* **73**, 76-83 (1980).

[5] R. Sanchez, S. Santandrea, "Convergence Analysis for the Method of Characteristics in Unstructured Mesh," Proc. M&C 2009, May 3-7, 2009, Saratoga (USA), on CD-ROM of this conference.

[6] R. Sanchez, L. Mao, S. Santandrea, 'Treatment of Boundary Conditions in Trajectory-Based Deterministic Unstructured Meshes,' *Nucl. Sci. and Eng.,* **64**, 384 (2000).

[7] S. Santandrea, R. Sanchez, P. Mosca "A Linear-Surface Approximation for Neutron Transport in Unstructured Meshes," *Nucl. Sci. and Eng.*, **160**, 1, p.23 (2008).